Homogeneous nucleation of NAD and NAT in liquid stratospheric aerosols: insufficient to explain denitrification

D. A. Knopf, T. Koop, B. P. Luo, U. G. Weers, T. Peter

Atmos. Chem. Phys. Discuss., 2, 669–687, 2002
www.atmos-chem-phys.org/acpd/2/669/

Atmospheric Chemistry and Physics Discussions

Homogeneous nucleation of NAD and NAT in liquid stratospheric aerosols: insufficient to explain denitrification

D. A. Knopf, T. Koop, B. P. Luo, U. G. Weers, and T. Peter

Institute for Atmospheric and Climate Science, Swiss Federal Institute of Technology, Zurich, Switzerland

Received: 18 April 2002 – Accepted: 13 May 2002 – Published: 12 June 2002

Correspondence to: D. A. Knopf (Daniel.Knopf@atmos.umnw.ethz.ch)

Abstract

The nucleation of NAD and NAT from HNO_3/H_2O and $HNO_3/H_2O/H_2SO_4$ solution droplets is investigated both theoretically and experimentally with respect to the formation of polar stratospheric clouds (PSCs). Our analysis shows that homogeneous NAD and NAT nucleation from liquid aerosols is insufficient to explain the number densities of large nitric acid containing particles recently observed in the Arctic stratosphere. This conclusion is based on new droplet freezing experiments employing optical microscopy combined with Raman spectroscopy. The homogeneous nucleation rate coefficients of NAD and NAT in liquid aerosols under polar stratospheric conditions derived from the experiments are $< 2 \times 10^{-5}$ $cm^{-3}\,s^{-1}$ and $< 8 \times 10^{-2}$ $cm^{-3}\,s^{-1}$, respectively. These nucleation rate coefficients are smaller by orders of magnitude than the value of $\sim 10^{3}$ $cm^{-3}\,s^{-1}$ used in a recent denitrification modelling study that is based on a linear extrapolation of laboratory nucleation data to stratospheric conditions (Tabazadeh et al., *Science*, *291*, 2591–2594, 2001). We show that this linear extrapolation is in disagreement with thermodynamics and experimental data and, therefore, must not be used in microphysical models of PSCs. Our analysis of the experimental data yields maximum hourly production rates of nitric acid hydrate particles per cm^3 of air of about 3×10^{-10} $cm^{-3}\,h^{-1}$ under polar stratospheric conditions. Assuming PSC particle production to proceed at this rate for two months we arrive at particle number densities of $< 5 \times 10^{-7}$ cm^{-3}, much smaller than the value of $\sim 10^{-4}$ cm^{-3} reported in recent field observations. This clearly shows that homogeneous nucleation of NAD and NAT from liquid supercooled ternary solution aerosols cannot explain the observed polar denitrification.

1. Introduction

Polar stratospheric cloud (PSC) particles activate chlorine from reservoir to reactive species by heterogeneous reactions on their surfaces. Measurements have shown that

ACPD

2, 669–687, 2002

PSCs can be composed of liquid supercooled ternary solutions (STS), nitric acid dihydrate (NAD), or nitric acid trihydrate (NAT) (Schreiner et al., 1999; Voigt et al., 2000). Large HNO_3-containing PSC particles can lead to significant denitrification of the polar stratosphere by sedimentation (Fahey et al., 2001). However, the mechanisms of how such large particles come about have not yet been established (Tolbert and Toon, 2001). It has been suggested that large nitric acid hydrate particles leading to denitrification could be produced by homogeneous nucleation of NAD and NAT from liquid STS (Tabazadeh et al., 2001), based on an extrapolation of laboratory aerosol nucleation data (Salcedo et al., 2001) to stratospheric conditions. However, the employed extrapolation is in disagreement with bulk nucleation experiments (Koop et al., 1995, 1997). To resolve these inconsistencies we investigate here the nucleation kinetics of NAD and NAT in liquid binary HNO_3/H_2O and ternary $HNO_3/H_2SO_4/H_2O$ solutions both theoretically and experimentally. First, we reexamine the physics of the nitric acid hydrate nucleation formulation used by Tabazadeh et al. (2001). Second, we present new experimental data on NAD and NAT nucleation from STS droplets under stratospheric conditions. Third, we use these data together with previously published data sets to deduce upper limits of homogeneous nucleation rate coefficients of NAD and NAT. Finally, from the inferred nucleation rate coefficients we derive maximum production rates of solid nitric acid particles under polar stratospheric conditions.

2. Nucleation formulation analysis

Salcedo et al. (2001) and Tabazadeh et al. (2001) have employed classical nucleation theory to describe the experimentally observed homogeneous nucleation rate coefficients, J_{hom}, of nitric acid hydrates (NAX; X = D or T):

$$J_{hom}(T) = n_{liq} \left(\frac{kT}{h}\right) \exp\left[\frac{-\Delta G_{act}(T)}{RT}\right] , \quad (1)$$

ACPD
2, 669–687, 2002

where n_{liq} is the HNO_3 molecular number density in the liquid, R is the universal gas constant, k is the Boltzmann constant, and h is the Planck constant. ΔG_{act} is the activation energy required to form a critical cluster in the solution. According to classical nucleation theory this activation energy depends on the saturation ratio of the respective nitric acid hydrate (S_{NAX}):

$$\Delta G_{act}(T) = \frac{16}{3}\pi\sigma_{sl}^3(T)\left[\frac{v_{sol}}{RT\ln(S_{\mathrm{NAX}})}\right]^2 + \Delta G_{dif}(T) \quad (2)$$

Here, σ_{sl} is the interfacial tension between the solid and liquid phase, v_{sol} is the molar volume of NAX in the critical cluster, and ΔG_{dif} is the HNO_3 diffusion activation energy across the boundary between the cluster and the solution. Since values for σ_{sl} and ΔG_{dif} are not available at stratospheric temperatures, ΔG_{act} can be determined from experimentally observed nucleation rate coefficients by solving Eq. 1 for ΔG_{act}:

$$\Delta G_{act}(T) = -RT\ln\left[\frac{h}{kT}\frac{J_{hom}(T)}{n_{liq}}\right] \quad (3)$$

Figure 1 shows values of ΔG_{act} in aqueous nitric acid solutions as plotted by Salcedo et al. (2001) as function of the NAD and NAT saturation ratio derived from their experimental data using Eq. (3). The laboratory data reveal a linear relationship between ΔG_{act} and S_{NAX} (solid lines in Fig. 1) in the experimentally observed range of saturation ratios (S_{NAD}=11–30, S_{NAT}=52–107). Since stratospheric saturation ratios (shaded areas in Fig. 1) are much smaller than the experimentally investigated range, Tabazadeh et al. (2001) used a linear extrapolation (dotted lines in Fig. 1) to infer ΔG_{act}-values for NAD and NAT at stratospheric conditions. However, applying such an extrapolation is physically unreasonable because according to Eq. (2), ΔG_{act} increases towards infinity for S_{NAX} approaching unity. In contrast, the linear extrapolation leads to a ΔG_{act}-value of about 30 kcal mol^{-1} in each case. Therefore, the linear extrapolation underestimates ΔG_{act} and, consequently, largely overestimates the homogeneous nucleation rate coefficient at low saturation ratios. In Fig. 2 we elucidate the effects of the linear extrapolation on the homogeneous nucleation rate coefficients of NAD and NAT in aqueous

nitric acid solutions. The nucleation formulation produces finite nucleation rate coefficients along the NAD and NAT melting point curves (where S_{NAX}=1) and does so even for values of $S_{NAX} < 1$ (not shown in Fig. 2). This is thermodynamically impossible for any spontaneous process, since the formation of an unstable crystal (similar to nucleating ice above 273.15 K) would lead to an increase of the total Gibbs free energy of the system. This nucleation formulation produces unrealistically high nucleation rate coefficients of about 10^8 cm^{-3} s^{-1} at the top of the NAD and NAT melting curves (dark yellow region at T = 230 K in Fig. 2a and T = 250 K in Fig. 2b) in disagreement with numerous experimental studies (Anthony et al., 1997; Koop et al., 1997; Bertram and Sloan, 1998a,b; Bertram et al., 2000; Salcedo et al., 2001). In addition, at stratospheric temperatures (180–200 K) and saturation ratios (between the solid and dotted lines in Fig. 2) the homogeneous nucleation rate coefficient increases with temperature. This behavior is due to the fact that in the formulation ΔG_{act} depends solely on S_{NAX}, independently of the temperature (Tabazadeh et al., 2001, note 21). Only in the proximity of the experimental data (black asterisks in Fig. 2) a reasonable temperature and concentration dependency of J_{hom} is observed. We conclude that the linear relationship between ΔG_{act} and S_{NAX} should not be used outside the range of available experimental data and, therefore, should not be extrapolated to stratospheric conditions.

3. Experimental

Freezing experiments with HNO_3/H_2O and $HNO_3/H_2SO_4/H_2O$ droplets were performed in order to determine homogeneous nucleation rate coefficients of NAD and NAT at stratospheric saturation ratios. We chose to investigate large droplets (0.12–0.27 cm in diameter) because smaller droplets (2×10^{-5}–8.5×10^{-3} cm in diameter) do not freeze at stratospheric temperatures and saturation ratios (Anthony et al., 1997; Bertram and Sloan, 1998a,b; Bertram et al., 2000; Salcedo et al., 2001). The droplets were deposited with a micropipette on a hydrophobically coated quartz plate inside a laminar flow clean bench. After sealing the droplets against ambient air with a second plate,

ACPD
2, 669–687, 2002

the aerosol cell was placed on a temperature stage attached to a Confocal Raman Microscope (see Fig. 3). In this setup the droplets' temperature can be varied between 170–295 K. The temperature was calibrated by measuring the melting points of heptane (182.55 K), octane (216.35 K), decane (243.45 K), dodecane (263.5 K), and water (273.15 K) in the cell. Phase changes (i.e. freezing or melting) are observed visually with the microscope part of the setup. In addition, the crystalline solids formed upon freezing were identified by Raman spectroscopy using a Nd:YAG-laser at a wavelength of 532 nm for illumination. The backscattered light is reflected onto a grating (1800 mm^{-1}) and focused on the CCD detector of the spectrograph. The resulting spectral resolution is about 2–4 cm^{-1} within the observed range of 500–4500 cm^{-1}. Figure 4 shows Raman spectra of droplets (10^{-2} cm^3) with an HNO_3:H_2O mole ratio of 1:2 and 1:3 corresponding to the stoichiometry of NAD and NAT, respectively. In each case the spectra were recorded during a cooling cycle (red spectra) and a warming cycle (blue spectra) at about the same temperature. To avoid any possible temperature bias the droplets were not illuminated by laser light during the course of the freezing experiments reported below. Spectra were taken only after the droplets were frozen.

Table 1 shows the composition of the investigated droplets. The droplets were prepared from stock solutions which were titrated against a 1 M NaOH solution. In an experimental run the droplets were cooled at a rate of $dT/dt = -10\,K\,min^{-1}$ until nucleation occurred. The ternary solution droplets (solution 3 and 4, Table 1) did not freeze above 178 K during such runs. Hence, the temperature in these experiments was decreased stepwise (by 5–10 K) keeping the temperature constant for several minutes after each step. All experiments were recorded on tape together with the experimental time and droplet temperature. The video tapes were analyzed afterwards to determine the number of nucleation events, n, as a function of time and temperature. The upper limit of the homogeneous nucleation rate coefficient J^{up}_{hom} can be derived from the

ACPD
2, 669–687, 2002

experimental data using the following formula:

$$J_{hom}^{up}(T) = \frac{n^*}{\sum_i V_i \cdot t_i(T)} \quad , \tag{4}$$

where $t_i(T) = \int_T^{T_i^*} (dT'/dt)_i^{-1} dT'$ is the time interval that the ith droplet with volume V_i remained liquid between T and T_i^*. T_i^* is either the nucleation temperature of the droplet or the lowest investigated temperature, and $(dT/dt)_i$ is the cooling rate applied in the particular experiment. n^* is the upper fiducial limit of n determined by Poisson statistics at a confidence level of 0.999 (Koop et al., 1997). Equation (4) yields a conservative (i.e. the highest possible) J_{hom}-value, which is in agreement with the experimental data.

In detail, Eq. (4) is conservative for the following reasons: First, the time interval, $t_i(T)$, that a droplet stays liquid below T is always smaller than the time interval it would stay liquid at T (assuming that J_{hom} monotonically increases with decreasing temperature in the investigated temperature range). Second, instead of using the actual number of nucleation events, n, we employed n^*, which represents a conservative value for n because $n^* > n$ in all cases. Third, it cannot be ruled out that heterogeneous nucleation of NAD and NAT occurred in the large droplets. Even in this case, the observed nucleation rate is always an upper limit for the homogeneous nucleation rate, independently of whether heterogeneous nucleation occurred or not. All experimental data were analyzed using Eq. (4). The derived J_{hom}^{up}-values were used to calculate lower limits of the activation energy, ΔG_{act}^{low}, according to Eq. (3).

4. Results and discussion

In Fig. 5 the resulting ΔG_{act}-values are shown as function of temperature and saturation ratio. The different symbols in Fig. 5 correspond to those in Table 1. In addition, we have reanalyzed published bulk experiments (Koop et al., 1995, 1997) to determine the upper limit for J_{hom} according to $J_{hom}^{up}(T) = n^*/(V \cdot t)$, where n^* is the same as

ACPD
2, 669–687, 2002

above, V is the volume of the solution, and t is the time the solution remained liquid at temperature T (Koop et al., 1997). The corresponding ΔG_{act}^{low}-values were obtained using Eq. (3) and are shown as open symbols in Fig. 5. The solid symbols in Fig. 5 represent the same data as in Fig. 1. Furthermore, we have added the aerosol nucleation data by Bertram et al. (2000). We note, that we have used a nucleation rate coefficient of $J = 4.4\times10^{9}$ cm^{-3} s^{-1} for these data, slightly lower than the one in the original publication (A.K. Bertram, personal communication). Figure 5 clearly reveals that the newly derived ΔG_{act}-values are significantly higher than the linear extrapolation formulation at stratospheric conditions. Since our data points are lower limits of ΔG_{act} (thus, upper limits of J_{hom}) the actual values of ΔG_{act} are likely to be even higher than those shown in Fig. 5. Clearly, the linear extrapolation used in Tabazadeh et al. (2001) is not in agreement with our new droplet data nor with bulk experiments published previously. In the following, we use the combined experimental data (Koop et al., 1995, 1997; Bertram and Sloan, 1998a,b; Bertram et al., 2000; Salcedo et al., 2001, and this work) to derive upper homogeneous nucleation rate coefficients of NAD and NAT at stratospheric conditions. Figure 6a shows the composition and corresponding NAD and NAT saturation ratios of STS droplets at 50 mbar (approx. 20 km altitude) for mixing ratios of 5 ppmv H_2O, 10 ppbv HNO_3, and 0.5 ppbv H_2SO_4 (Carslaw et al., 1994). In Fig. 6b, NAD and NAT nucleation rate coefficients are shown for the conditions displayed in panel (a). In the region of highest saturation ratios (shaded region in Fig. 6) circles and squares represent maximum nucleation rate coefficients derived from experimental data as follows: In Fig. 5 for one temperature (e.g. 191.5 K) all data points are selected by color, and then interpolated as function of saturation ratio using S_{NAX} read off Fig. 6a. From the ΔG_{act}-value obtained in this way we derive J_{hom}^{up} using Eq. (1). Blue and red arrows mark the temperature where S_{NAD}=1 and S_{NAT}=1, respectively, i.e. where the nucleation rate coefficients must decrease to zero. Solid lines in Fig. 6b represent homogeneous nucleation rate coefficients calculated using the formulation of Tabazadeh et al. (2001). Figure 6c shows the corresponding NAD and NAT particle production rates for the conditions displayed in panel (a) using the nucleation

ACPD
2, 669–687, 2002

rate coefficients shown in panel (b). Solid lines are calculated with the equations given by Tabazadeh et al. (2001) taking into account that the total aerosol volume increases with decreasing temperature (Carslaw et al., 1994). Stars are values taken directly from Fig. 1 in Tabazadeh et al. (2001). The circles and squares represent the production rates calculated using the experimentally derived upper nucleation rate coefficients shown in Fig. 6b. Figure 6c reveals that the maxima of the resulting production rates of the formulation by Tabazadeh et al. (2001) (solid lines) are too large by a factor of 10^8 for NAD and 10^4 for NAT when compared to the experimentally derived production rates.

5. Conclusions

Salcedo et al. (2001) have investigated the nucleation of NAD and NAT from binary aqueous nitric acid droplets. We consider their experimental data to be sound and the observed linear relationship between the activation energy, ΔG_{act}, and the respective nitric acid hydrate saturation ratio, S_{NAX}, to be valid in the experimentally observed range of saturation ratios (S_{NAD}=11–30, S_{NAT}=52–107). However, the theoretical arguments and experimental data presented above show that the linear relationship between ΔG_{act} and S_{NAX} is not valid at stratospheric saturation ratios. Therefore, the linear relationship must not be used in microphysical models of PSCs.

The analysis of experimental data presented above shows homogeneous NAD and NAT nucleation rate coefficients to be exceedingly low ($< 2 \times 10^{-5}$ cm^{-3} s^{-1} and $< 8 \times 10^{-2}$ cm^{-3} s^{-1}, respectively) in STS aerosols under polar stratospheric conditions, in agreement with earlier studies (Koop et al., 1995, 1997). These nucleation rate coefficients are smaller by orders of magnitude than those used in a recent modelling study of stratospheric denitrification (Tabazadeh et al., 2001). In that study, it was asserted that homogeneous NAD and NAT nucleation from STS aerosols is sufficient to explain the denitrification observed in the Arctic and Antarctic stratosphere. NAT particle number densities that are in agreement with recent field observations ($\sim 10^{-4}$ cm^{-3}, Fahey

et al., 2001) were obtained by converting all NAD particles into NAT particles in the simulation. This was achieved by adding the NAD and NAT homogeneous nucleation rate coefficients. The corresponding particle production rates were about $\sim 10^{-5}$ cm^{-3} h^{-1}. In contrast, using the upper limits for the particle production rates (Fig. 6c) derived in this study and assuming the maximum saturation ratios to persist for two months, we arrive at particle number densities of $\sim 5 \times 10^{-7}$ cm^{-3}, much smaller than reported by Fahey et al. (2001). Furthermore, Tabazadeh et al. (2001) state that NAT particle production rates smaller than $\sim 10^{-5}$ cm^{-3} h^{-1} are unimportant to denitrification. Even if we combine the NAD and NAT production rates of Fig. 6c the maximum possible value in agreement with the laboratory data is only $\sim 3{\times}10^{-10}$ cm^{-3} h^{-1}. This clearly shows that homogeneous nucleation of NAD and NAT from liquid supercooled ternary solution aerosols cannot explain the observed polar denitrification.

Acknowledgements. We are grateful to D. Salcedo and A. K. Bertram for providing original experimental data sets. Internal funding through an ETH grant is gratefully acknowledged.

References

Anthony, S. E., Onash, T. B., Tisdale, R. T., Disselkamp, R. S., Tolbert, M. A., and Wilson, J. C.: Laboratory studies of ternary $HNO_3/H_2SO_4/H_2O$ particles: Implications for polar stratospheric cloud formation, J. Geophys. Res., 102, 10 777–10 784, 1997. 673

Bertram, A. K. and Sloan, J. J., Temperature-dependent nucleation rate constants and freezing behavior of submicron nitirc acid dihydrate aerosol particles under stratospheric conditions, J. Geophys. Res., 103, 3553–3561, 1998a. 673, 676, 682, 686

Bertram, A. K. and Sloan, J. J.: The nucleation rate constants and freezing mechanism of nitric acid trihydrate aerosol under stratospheric conditions, J. Geophys. Res., 103, 13 261–13 265, 1998b. 673, 676, 682, 686

Bertram, A. K., Dickens, D. B., and Sloan, J. J.: Supercooling of type 1 polar stratospheric clouds: The freezing of submicron nitirc acid aerosols having HNO_3 mole fractions less than 0.5, J. Geophys. Res., 105, 9283–9290, 2000. 673, 676, 686

Carslaw, K. S., Luo, B. P., Clegg, S. L., Peter, T., Brimblecombe, P., and Crutzen, P. J.: Stratospheric aerosol growth and HNO_3 gas phase depletion from coupled HNO_3 and water uptake by liquid particles, Geophys. Res. Lett., 21, 2479–2482, 1994. 676, 677, 687

Fahey, D. W., Gao, R. S., Carslaw, K. S., Kettleborough, J., Popp, P. J., Northway, M. J., Holecek, J. C., Ciciora, S. C., McLaughlin, R. J., Thompson, T. L., Winkler, R. H., Baumgardner, D. G., Gandrud, B., Wennberg, P. O., Dhaniyala, S., McKinney, K., Peter, T., Salawitch, R. J., Bui, T. P., Elkins, J. W., Webster, C. R., Atlas, E. L., Jost, H., Wilson, J. C., Herman, R. L., Kleinböhl, A., and von König, M.: The Detection of Large HNO_3-Containing Particles in the Winter Arctic Stratosphere, Science, 291, 1026–1030, 2001. 671, 677, 678

Koop, T., Biermann, U. M., Raber, W., Luo, B. P., Crutzen, P. J., and Peter, T.: Do stratospheric aerosol droplets freeze above the ice frost point?, Geophys. Res. Lett., 22, 917–920, 1995. 671, 675, 676, 677, 686

Koop, T., Luo, B. P., Biermann, U. M., Crutzen, P. J., and Peter, T., Freezing of $HNO_3/H_2SO_4/H_2O$ Solutions at Stratospheric Temperatures: Nucleation Statistics and Experiments, J. Phys. Chem. A, 101, 1117–1133, 1997. 671, 673, 675, 676, 677, 686

Salcedo, D., Molina, T., and Molina, M. J.: Homogeneous Freezing of Concentrated Aqueous Nitric Acid Solutions at Polar Stratospheric Temperatures, J. Phys. Chem. A, 105, 1433–1439, 2001. 671, 672, 673, 676, 677, 682, 686

Schreiner, J., Voigt, C., Kohlmann, A., Arnold, F., Mauersberger, K., and Larson, N.: Chemical

Analysis of Polar Stratospheric Cloud Particles, Science, 283, 968–970, 1999. 671
Tabazadeh, A., Jensen, E. J., Toon, O. B., Drdla, K., and Scheberl, M. R.: Role of the Stratospheric Polar Freezing Belt in Denitrification, Science, 291, 2591–2594, 2001. 671, 672, 673, 676, 677, 678, 682, 683, 686, 687
Tolbert, M. A. and Toon, O. B., Solving the PSC Mystery, Science, 292, 61–63, 2001. 671
Voigt, C., Schreiner, J., Kohlmann, A., Zink, P., Mauersberger, K., Larsen, N., Deshler, T., Kröger, C., Rosen, J., Adriani, A., Cairo, F., di Donfrancesco, G., Viterbini, M., Ovarlez, J., Ovarlez, H., David, C., and Dörnback, A.: Nitric Acid Trihydrate (NAT) in Polar Stratospheric Clouds, Science, 290, 1756–1758, 2000. 671

Table 1. Composition and volume of investigated droplets. The symbols refer to the ones in Fig. 5

Solution	HNO_3 [wt%]	H_2SO_4 [wt%]	H_2O [wt%]	Volume [$10^{-3}cm^{-3}$]	Symbol
1	63.6	0	36.4	5–10	×
2	53.8	0	46.2	1–10	+
3	32.2	13.8	54.0	10	*
4	38.3	7.6	54.1	10	•

ACPD
2, 669–687, 2002

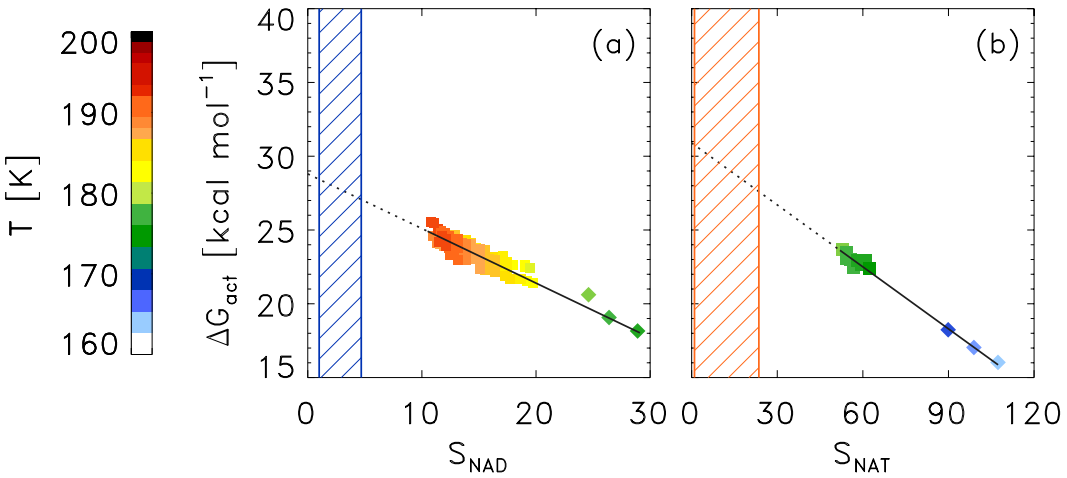

Fig. 1. ΔG_{act} as function of the NAD and NAT saturation ratios derived from laboratory nucleation data using Eq. (3) (Salcedo et al., 2001). All data points were derived from experiments with droplets consisting of binary aqueous nitric acid solutions of varying composition. **(a):** ■: 57 wt%, 60 wt%, and 64 wt% HNO_3 (Salcedo et al., 2001); ♦: 64 wt% HNO_3 (Bertram and Sloan, 1998a). **(b):** ■: 54 wt% HNO_3 (Salcedo et al., 2001); ♦: 54 wt% HNO_3 (Bertram and Sloan, 1998b). The color coding indicates at which temperature the data were obtained. The shaded regions indicate typical NAD and NAT saturation ratios at polar stratospheric conditions. The solid lines show the linear relationship between ΔG_{act} and S_{NAX} observed by Salcedo et al. (2001), and the dotted lines are the linear extrapolations to stratospheric conditions used in Tabazadeh et al. (2001).

ACPD
2, 669–687, 2002

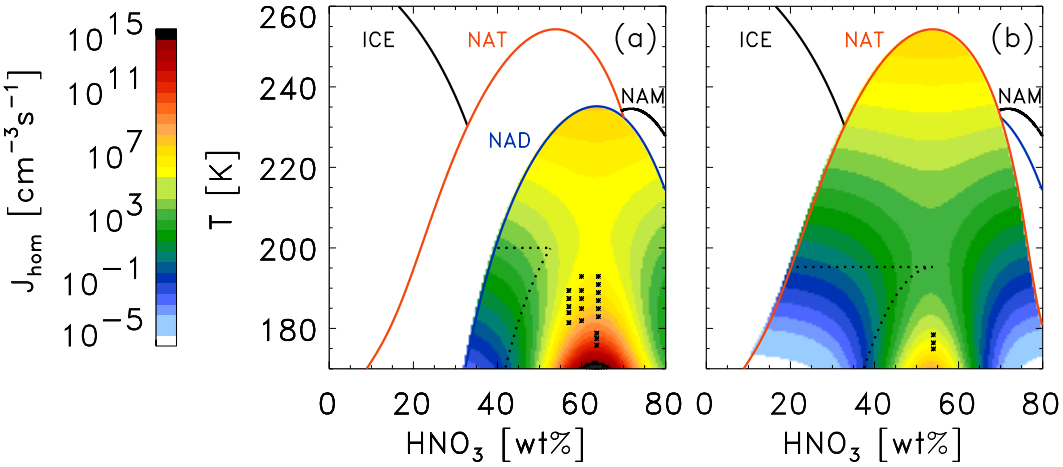

Fig. 2. Homogeneous nucleation rate coefficients of NAD (a) and NAT (b) in binary HNO_3/H_2O solutions as function of temperature and concentration using the formulation of Tabazadeh et al. (2001). Solid lines show the melting point curves of the different solid phases (S = 1). The regions between dotted and solid lines indicate typical polar stratospheric temperatures (≤ 200 K) and saturation ratios (≤ 4.7 for NAD and ≤ 23.5 for NAT). Black asterisks correspond to the experimental data shown in Fig. 1.

ACPD
2, 669–687, 2002

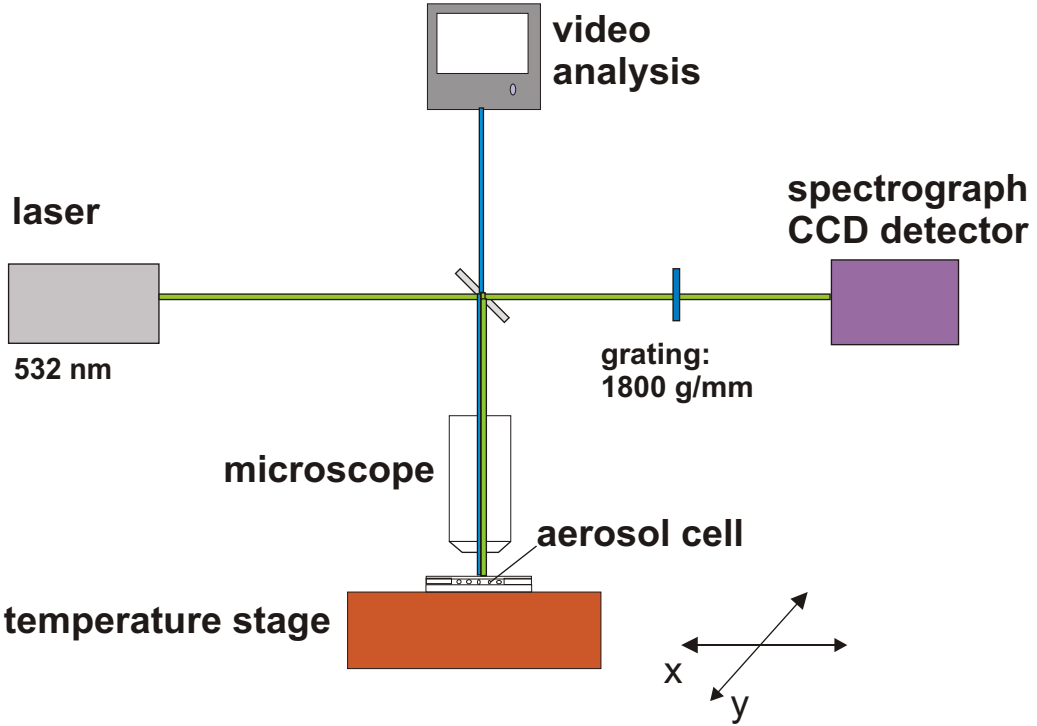

Fig. 3. Sketch of the experimental setup.

ACPD
2, 669–687, 2002

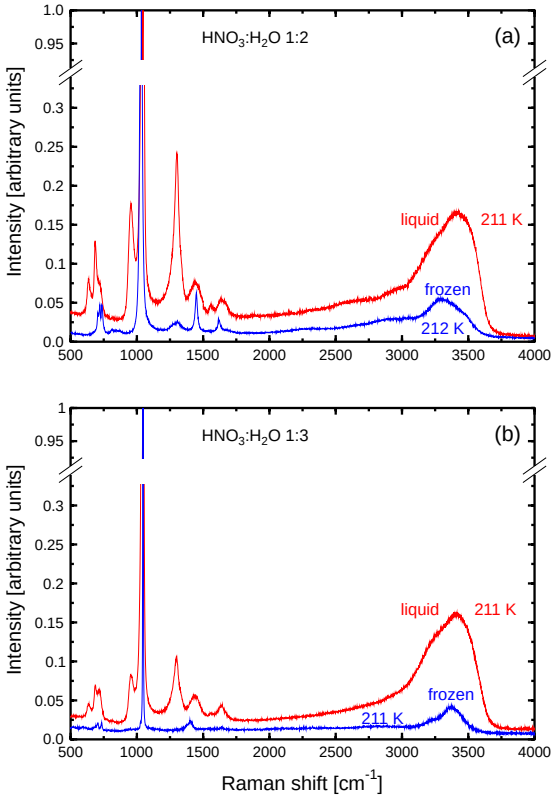

Fig. 4. Raman spectra of droplets with a volume of 10^{-2} cm^3. **(a):** Red line: spectrum of a liquid droplet with a HNO_3:H_2O mole ratio of 1:2 at 211 K; blue line: spectrum of a frozen droplet at 212 K. **(b):** Red line: spectrum of a liquid droplet with a HNO_3:H_2O mole ratio of 1:3 at 211 K; blue line: spectrum of a frozen droplet at 211 K. The spectra are normalized with respect to the $\nu_1(NO_3^-)$ vibration band at ~1040 cm^{-1}.

ACPD
2, 669–687, 2002

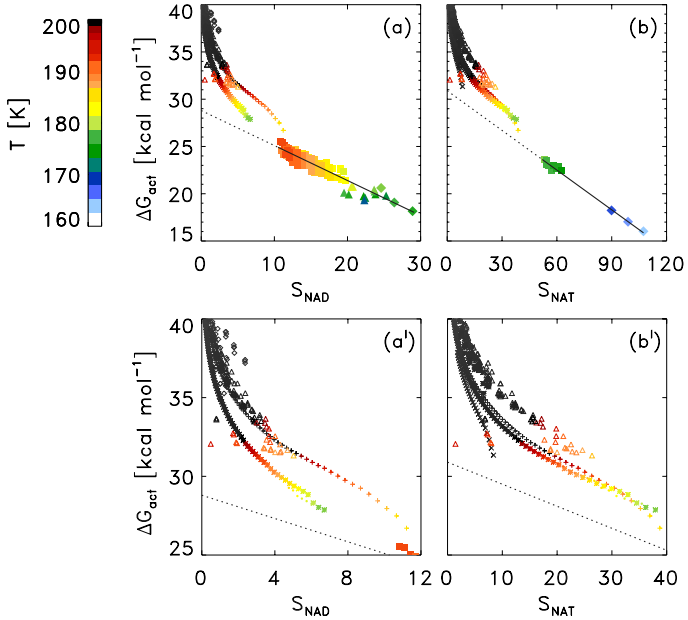

Fig. 5. ΔG_{act} as function of the NAD and NAT saturation ratios derived from laboratory nucleation data using Eq. 3. Large droplet data: ×: 63.6 wt% HNO_3; +: 53.8 wt% HNO_3; ∗: 32.2 wt% HNO_3 and 13.8 wt% H_2SO_4; •: 38.3 wt% HNO_3 and 7.6 wt% H_2SO_4 (all this work). Bulk solution data: △: binary HNO_3/H_2O solutions of varying composition (Koop et al., 1997). ◊: ternary $HNO_3/H_2SO_4/H_2O$ solutions of varying composition (Koop et al., 1995, 1997). Aerosol data: **(a):** ■: 57 wt%, 60 wt%, and 64 wt% HNO_3 (Salcedo et al., 2001); ♦: 64 wt% HNO_3 (Bertram and Sloan, 1998a); ▲: binary HNO_3/H_2O aerosol of varying composition (Bertram et al., 2000). **(b):** ■: 54 wt% HNO_3 (Salcedo et al., 2001); ♦: 54 wt% HNO_3 (Bertram and Sloan, 1998b). The color coding indicates at which temperature the data were obtained. The solid lines indicate the linear relationship between ΔG_{act} and S_{NAX} observed by Salcedo et al. (2001), and the dotted lines are the linear extrapolations to stratospheric conditions used in Tabazadeh et al. (2001). **(a')** and **(b')** show an enlarged view of the top left corner of panels **(a)** and **(b)**, respectively.

ACPD
2, 669–687, 2002

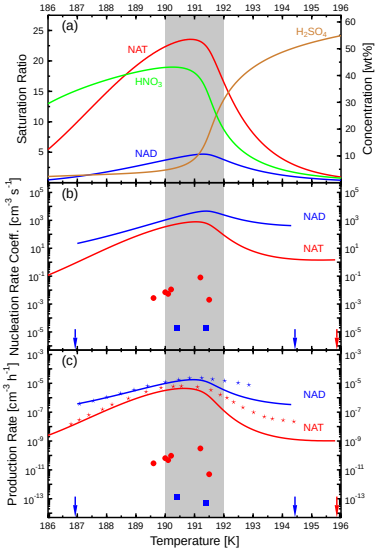

Fig. 6. **(a)** The composition (green and orange lines) and the saturation ratios (red and blue lines) of STS aerosols as a function of temperature at 50 mbar with 5 ppmv H_2O, 10 ppbv HNO_3, and 0.5 ppbv H_2SO_4 (Carslaw et al., 1994). The shaded region indicates the temperature range where the S_{NAX}-values have their maximum. **(b):** Upper limits for the nucleation rate coefficients of NAD (squares) and NAT (circles) in STS droplets, derived from experimental data for the conditions shown in panel (a). For comparison, solid lines indicate the homogeneous nucleation rate coefficient in STS droplets for the same conditions calculated using the formulation of Tabazadeh et al. (2001). **(c):** Hourly production rates of NAD and NAT particles (squares and circles, respectively) per cm^3 of air derived from the nucleation rate coefficients shown in panel (b). The increase of the total aerosol volume with decreasing temperature was taken into account (Carslaw et al., 1994). Also shown as solid lines are the NAD and NAT production rates for the same conditions calculated using the formulation of Tabazadeh et al. (2001). Stars show values for similar conditions taken directly from Fig. 1 of Tabazadeh et al. (2001). (We note that we can reproduce the stars by assuming a constant total aerosol volume of 5.9×10^{-12} cm^3.) Arrows in (b) and (c) mark the temperature where the saturation ratio of NAD (blue) and NAT (red) equals one.

ACPD
2, 669–687, 2002